Efficient Deep Learning Ensemble for Skin Lesion Classification

David Dueñas Gaviria[1] [a], Md Mostafa Kamal Saker[2] [b] and Petia Radeva[3,4] [c]

[1]*Facultat d'Informatica de Barcelona, Universitat Politècnica de Catalunya, Carrer de Jordi Girona 31, Barcelona, Spain*

[2]*Department of Engineering Science, University of Oxford, Headington OX3 7DQ, Oxford, England, U.K.*

[3]*Department of Mathematics and Computer Science, Universitat de Barcelona, Gran Via de les Corts Catalanes 585, Barcelona, Spain*

[4]*Computer Vision Center, Bellaterra, Barcelona, Spain*

Keywords: Skin Cancer, Melanoma, ISIC Challenge, Vision Transformers.

Abstract: Vision Transformers (ViTs) are deep learning techniques that have been gaining in popularity in recent years. In this work, we study the performance of ViTs and Convolutional Neural Networks (CNNs) on skin lesions classification tasks, specifically melanoma diagnosis. We show that regardless of the performance of both architectures, an ensemble of them can improve their generalization. We also present an adaptation to the Gram-OOD* method (detecting Out-of-distribution (OOD) using Gram matrices) for skin lesion images. Moreover, the integration of super-convergence was critical to success in building models with strict computing and training time constraints. We evaluated our ensemble of ViTs and CNNs, demonstrating that generalization is enhanced by placing first in the 2019 and third in the 2020 ISIC Challenge Live Leaderboards (available at https://challenge.isic-archive.com/leaderboards/live/).

1 INTRODUCTION

Skin cancer has become a major public health concern; between 2 and 3 million non-melanoma skin cancers occur each year and 132 thousand melanoma worldwide, claiming more than 20 thousand lives in Europe alone each year, and 57 thousand worldwide, based on the most recent (Forsea, 2020), (ACS, 2022). Melanoma is the deadliest form of skin cancer (WHO, 2017), and a later stage of melanoma diagnosis has been linked to a significant increase in mortality rate.

As medical professionals and patients' needs for technology have increased, so have the demands for automated skin cancer diagnosis (Chang et al., 2013). In response, current research has produced automated skin cancer diagnostic tools that perform on par with dermatologists who rely mostly on visual diagnosis, dermoscopic analysis, or invasive biopsy, along with a histopathological study. Nonetheless, Deep Learning (DL) has revolutionized the field of computer vision in recent years with the resurgence of Neural Network (NNs) architectures (Belilovsky et al., 2019). Convolutional Neural Networks (CNNs) have become the dominant DL technique in this field, due in large part to their success in the ImageNet Large Scale Visual Recognition Challenge (ILSVRC) (Russakovsky et al., 2015). However, there are a number of other DL techniques that have been gaining in popularity in recent years. Particularly, Vision Transformers (ViTs) (Dosovitskiy et al., 2021), which correspond to a type of transformer that is specifically designed for computer vision tasks. Transformers are a type of DL model based on the attention mechanism and have proved successful in a number of natural languages processing tasks (Vaswani et al., 2017). Although considerable research has been done on the use of ViTs for medical image classification, see (Chen et al., 2021; Sarker et al., 2022), robustness against skin lesions in generalization has not yet been explicit. This is generally the case because the training and testing data for many closed-world tasks are taken from the same distribution. However, in the ISIC 2019 dataset particularly, the effect of an outlier class poses a significant challenge for ViTs in comparison to traditional CNNs. Hence, the aim of this study is to answer: How useful is the incorporation of ViTs in classification for skin cancer detection, particularly melanoma, in comparison to CNNs?

Skin lesion classification using ViTs and CNNs

[a] https://orcid.org/0000-0002-4869-668X
[b] https://orcid.org/0000-0002-4793-6661
[c] https://orcid.org/0000-0003-0047-5172

Gaviria, D., Saker, M. and Radeva, P.
Efficient Deep Learning Ensemble for Skin Lesion Classification.
DOI: 10.5220/0011816100003417
In *Proceedings of the 18th International Joint Conference on Computer Vision, Imaging and Computer Graphics Theory and Applications (VISIGRAPP 2023) - Volume 5: VISAPP*, pages 303-314
ISBN: 978-989-758-634-7; ISSN: 2184-4321

shares the same goal of detecting skin disease lesions by using image-level and patient-level data. Thus, it makes sense to test their performance together using a common ensemble. As a result, the contributions of this study are as follows:

- Focusing on the main goal of skin disease classification problem, we propose a robust model, based on an ensemble comprising a wide range of model architectures, including top accuracy ViTs and popular CNNs. Our model outperformed the state of the art in the 2019 ISIC competition.
- Instead of using a loss function normalized to take into account imbalanced data during the training, our model demonstrates that the skin lesion diagnosis represented by its inherent imbalanced data can be handled by re-scaling the decision threshold at model inference.
- Our model shows improvements in the Gram-OOD* method for the detection of OOD samples in the ensemble predictions.
- We employed the super-convergence phenomenon which allowed for a larger number of individual experiments, despite computing and time constraints.
- Finally, providing a consistent validation pipeline, we demonstrate that applying domain-dependent transformations is crucial in a data augmentation regime achieving top performance with our combined ViTs and CNNs ensemble model.

The following study is arranged as follows: Section 2 goes over our model description and implementation processes training various ViTs and CNNs models used along with details on the data used. Section 3 displays and summarizes the results acquired along with the discussion on the validation approach. Finally, last section gives conclusions of the study given and future research lines to be pursued.

2 METHODOLOGY

Here we introduce our new method for skin lesion classification, which was able to demonstrate robustness in generalization by scoring first in the 2019 ISIC Challenge and third in the 2020 ISIC Challenge, despite computing and training-time limitations. Overall, the following contributions made it possible to achieve such a position: a diversity provided by ViTs and CNNs ensemble; handling the imbalanced data problem, through re-scaling the model's predictions, by using the output class probabilities; improvements in OOD detection through an adaptation of the Gram-OOD* method; super-convergence through the usage of OneCycle LR in conjunction with AdamP optimizer, and domain-dependent image augmentation, for learning credible representations of skin lesions.

2.1 A New Ensemble of Deep Learning Models for Skin Lesion Classification

A variety of state-of-the-art ViTs and CNNs were explored in our work in order to study their jointly behaviour in the context of skin lesion diagnosis. After a thorough analysis on the state-of-the-art DL models, we concluded that the highly complex problem of skin lesion classification requires an ensemble of robust performing models. Hence, here we propose an ensemble that consists of:

- Data-efficient Image Transformer (DeiT) (Touvron et al., 2021a) - a type of ViT trained using a teacher-student strategy specific to transformers relying on a distillation token, it ensures that the student learns from the teacher through attention.
- EfficientNets (Tan and Le, 2019), trained on Noisy-Student weights (Xie et al., 2020) and using a scaling technique to equally scale the network's width, depth, and resolution using a set of predefined scaling coefficients.
- ConvNeXt (Liu et al., 2022b), resulting in a hybrid model lacking attention-based modules that adapt a ConvNet towards the design of a hierarchical Swin transformer.

The diagram of the pipeline is depicted in Figure 1, which shows the use of both ViTs and CNNs. Thus, the final ensemble in the training pipeline (a) shows in blue and green the CNNs and ViTs respectively, being trained using the dataset images with the external datasets (see Figure 4). The orange line, on the other hand, represents the pipeline that was used to train the network to add the metadata. Afterwards, model selection is performed at the training phase, determining the correlation of each model's training and validation prediction to filter out overfitting models. (b) indicates the inference pipeline, which consisted of generating output predictions using Test Time Augmentation (TTA) (Shanmugam et al., 2020) with a similar augmentation regime than in training (Except CutOut). Moreover, creating the ensemble by averaging the model predictions and performing thresholding on the resulting predictions. Finally, Gram-OOD* adaptation improves OOD detection by replacing the method's generated outlier class predictions in the previous ensemble.

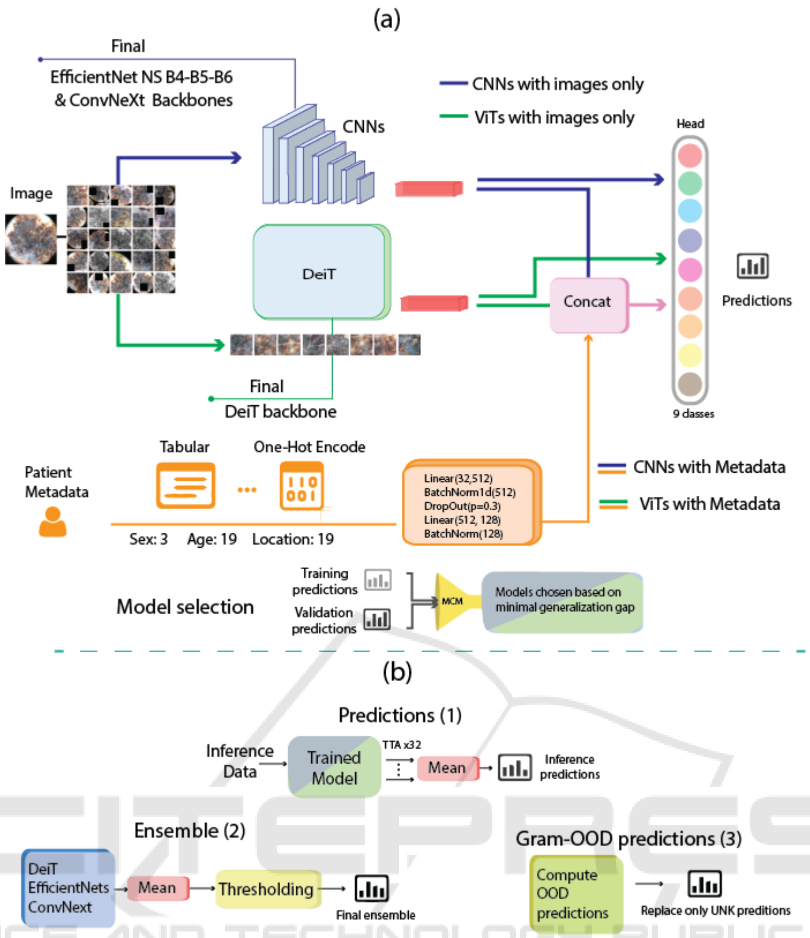

Figure 1: Diagram of the pipeline of our model. (a) depicts the training pipeline and (b) inference pipeline. The final ensemble uses an average of models trained with only images, and both images and metadata. The inference pipeline shows the output predictions in three stages.

2.2 Model Selection Based on Mean Correlation Matrix

The goal of our strategy inspired in (Nikita Kozodoi, 2020) is to exclude models whose mean correlation of predictions revealed a significant gap between training and validation predictions among the different models in order to select consistent and stable models. The basic idea is to find the correlation between the training predictions and in the correlation of the validation predictions for the individual models to assess the divergence between training and validation based on the correlations of each pair of models. Equations (1) and (2) indicate the correlation coefficients ρ^{ij} for each pair of models i and j forming a stacked matrix for the training x_{tr} and validation x_v data:

$$\rho_{tr}^{ij} = \sum_{c=1}^{|C|} \frac{\sum_{k=1}^{|c|}(x_{tr,k}^{i} - \mu_{tr,c}^{i})(x_{tr,k}^{j} - \mu_{tr,c}^{j})}{\sigma_{tr,c}^{i} * \sigma_{tr,c}^{j}} \qquad (1)$$

$$\rho_{v}^{ij} = \sum_{c=1}^{|C|} \frac{\sum_{k=1}^{|c|}(x_{v,k}^{i} - \mu_{v,c}^{i})(x_{v,k}^{j} - \mu_{v,c}^{j})}{\sigma_{v,c}^{i} * \sigma_{v,c}^{j}}, \qquad (2)$$

where $x_{tr,k}^{i}$ are the training data output of model i of class c, $x_{v,k}^{i}$ are the validation data output of model i of class c, $\mu_{tr,c}^{i}$ and $\sigma_{tr,c}^{i}$ are the mean and the variance of the training data output of model i of class c, $\mu_{v,c}^{i}$ and $\sigma_{v,c}^{i}$ are the mean and the variance of the validation data output of model i of class c, $|C|$ is the number of classes and $|c|$ is the number of data in class c.

Equation (3) shows the Mean Correlation Matrix (MCM) which corresponds to the arithmetic mean computation of the absolute gap difference of the model-pair-wise correlations:

$$\{MCM^{ij}\} = \left|\rho_{v}^{ij} - \rho_{tr}^{ij}\right|. \qquad (3)$$

Note that the MCM matrix has dimensions $|M| \times |M|$ where $|M|$ is the number of models. In order to find the first T models with minimum gap, we sum the differences corresponding to each model (summing the rows of the MCM matrix), sort them and keep the first T models with minimum values:

$$\{sort\{\frac{1}{|M|}\sum_{i=1}^{|M|} MCM^{ij}\}\}_{j=1,\dots,T}.$$

Note that a greater gap MCM indicates that the model predictions behave differently between training and validation data. Therefore, it is possible that a feature on which this model largely depends, has a different distribution between training and validation data, causing it to overfit the training data and affect its generalization. Section 3.6 proves the importance of the MCM in the ensemble's model selection.

2.3 OOD with a Modified Gram-OOD*

Gram-OOD (Sastry and Oore, 2019) is a robust approach that relies on intermediate feature activations to treat data with OOD samples, with the benefit of not requiring additional data. In order to detect abnormalities, the original method computes layer-wise correlations using Gram-Matrices:

$$G_l^p = F_l^p F_l^{p\top}, \qquad \Delta(\check{x}) = \sum \frac{\delta_l(\check{x}_c)}{E_v[\delta_l]}. \tag{4}$$

where c corresponds to the class assigned by the classifier, $\check{x}$ represents the total deviation of a new image, F_l corresponds to the activation of layer l, L - the total number of layers, p is a parameter, $E_v[\delta_l]$ is the expected deviation from the validation data at layer δ_l. In other words, to highlight the prominent features, Equation (4) computes high-order Gram-Matrices of order p with F_l corresponding to activations at layer l. The first step is to compute the pair-wise correlation between the obtained feature maps, both in convolutional layers and activation layers. Next, the layer-wise deviations from the gram matrices are computed so that it is possible to know how much a sample deviates from the max/min values over the training data. Finally, the original method computes the total deviation by summing its layer-wise deviation across all layers. In Equation (4), the expected deviation from the validation data $E_v[\delta_l]$ is computed using the validation set, avoiding the need for OOD datasets, in contrast to techniques such as (Liang et al., 2018), which need both in-distribution and OOD datasets.

The Gram-OOD* (Pacheco et al., 2020) considers only the activation layers adding an extra normalizing layer between the pair-wise correlations and the layer-wise variances. The normalization procedure is:

$$\tilde{G_l^p} = \frac{\hat{G_l^p} - min(\hat{G_l^p})}{max(\hat{G_l^p}) - min(\hat{G_l^p})} \tag{5}$$

In this paper, we propose a modified version of the Gram-OOD* (Pacheco et al., 2020) in which the feature maps are computed from the convolutional layers, instead of the activation layers. In this way, we retain critical features from the pair-wise correlations and apply the normalization procedure (see Equation (5)) with a substantially reduced computational cost without sacrificing generalization capacity.

2.4 Loss Function for Skin Lesion Classification

As in many medical image datasets, data imbalance is a common, yet challenging issue to be addressed for model design and hyper-parameters optimization. Most popular approaches, such as Weighted Cross Entropy (WCE) (Aurelio et al., 2019), or Focal loss (FL) (Lin et al., 2020) have been widely used to address it. However, performance can improve by means of the regular Cross Entropy (CE) properly re-scaling the output predictions at inference as follows:

$$CE = -\sum_{c=1}^{|C|} y_{o,c} \log(p_{o,c}) \tag{6}$$

where $|C|$ is the number of classes, y as the binary indicator (groundtruth) if class label c is correct for observation o, and p is the predicted probability observation that o is of class c. The improvement is achieved by re-scaling the output class probabilities with the method known as thresholding (Buda et al., 2018). This approach applied in (Steppan and Hanke, 2021) has been demonstrated to significantly improve the performance in imbalanced datasets by a class probability distribution approximation. (Richard and Lippmann, 1991) has shown that NNs classifiers derive Bayesian a posteriori probabilities, where they are computed for each class by their frequency in the imbalanced dataset. In other words, the threshold $T(x)$ is computed given the output for class c for a datapoint x that implicitly corresponds to the conditional probability in Equation (7), where $|c|$ is the number of unique training and validation instances in class c and $p(x)$ is considered constant assuming all data have the same probability to be selected:

$$T(x) = p(c|x) = \frac{p(c)p(x|c)}{p(x)}, \; p(c) = \frac{|c|}{\sum_{k=1}^{|C|} |c_k|}, \tag{7}$$

where $p(x|c)$ is the output of the softmax layer and $|c_k|$ is the number of instances of class c_k. Thus, depending on the datasets that are considered, the re-scaling made by the class prior will change.

3 VALIDATION

In this section, we discuss the datasets and their preparation, followed by the main ensemble setting, and evaluation metrics. Furthermore, we illustrate the experimental results and discussions showing the effect of the super-convergence, data augmentation, OOD and the imbalanced data methods followed by the final results on both challenges datasets from ISIC 2019 and ISIC 2020.

3.1 Skin Lesion Dataset Description

At the image level, there are 9.1 GB worth 25,331 dermoscopic images available for training in 8 different classes. This information was obtained from the Memorial Sloan Kettering Cancer Center, the BCN_20000 dataset from the Department of Dermatology, Hospital Clinic de Barcelona (Combalia et al., 2019) and the HAM10000 dataset from the Department of Dermatology, Medical University of Vienna (Tschandl et al., 2018). Table 1 shows the nine classes used for the diagnosis in the challenge and Table 2 shows the distribution of the external datasets. Likewise, the test dataset comprised 8,239 images with the extra outlier class that was not represented in the training data. Aside from the images, the collection includes metadata such as the patient's age and sex as well as the location of the individual skin lesion.

ISIC 2020 dataset (Rotemberg et al., 2021) is composed of 23 GB worth 33,126 images of different resolutions for training and 10982 for the test set. A total of 2056 patients was gathered for this dataset at various locations around the world. In contrast to the 2019 dataset, the unknown class (UNK) accounted for the majority of benign occurrences, including Cafe-au-lait macule and atypical melanocytic proliferation diagnosis, whereas the other three: melanocytic nevus (NV), melanoma (MEL), and benign keratosis (BKL), were also shared diagnosis within the 2019 dataset; the Basal cell carcinoma (BCC), Actinic keratosis (AK), Squamous cell carcinoma (SCC), Vascular lesion (VASC) and Dermatofibroma (DF) are unique diagnosis from the 2019 dataset.

With the presence of an outlier class in the ISIC 2019 dataset, it was reasonable to experiment with external data to attempt to increase training diversity for the unknown and generalization of the remaining classes. As an outline of (Steppan and Hanke, 2021), the outlier class for training was addressed through the usage of a subset of a collection of datasets, which are shown in Table 2.

Table 1: Diagnosis distribution of 2019 and 2020 ISIC datasets.

Diagnosis	2019 dataset samples	2020 dataset samples
NV	12875 (50%)	5193 (15%)
MEL	4522 (18%)	584 (2%)
BKL	2624 (10%)	223 (1%)
UNK	0 (0%)	27126 (82%)
BCC	3323 (13%)	—
AK	867 (4%)	—
SCC	628 (3%)	—
VASC	253 (1%)	—
DF	239 (1%)	—
Total	25331	33126

Table 2: Diagnosis distribution for the external dataset.

External data					
Dataset	7 point (Walter et al., 2013)	PH2 (Giotis et al., 2015)	MED-NODE (Giotis et al., 2015)	SD-198 (Sun et al., 2016)	Total
Number of images	1011 (13%)	200 (3%)	170 (2%)	5944 (78%)	7624
Total	7624				

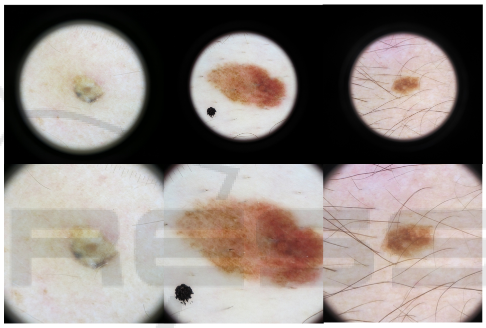

Figure 2: Preprocesssing of outlier images.

3.2 Data Preparation

The images in the dataset are all from different sources, scanned at various resolutions and on the same color space. However, some of them are composed of microscope-like image cropping that were detected as outliers, using the mean and standard deviation from the intensity values, and were preprocessed to see whether they could result in an generalized improvement as (Gessert et al., 2020) stated. The data handling first consisted of trimming and cropping these microscope-lesion images, which were typically high resolution. This process resulted in another image with a lower resolution than the original, but with the object of interest (skin lesion) clearly visible and in greater detail. Figure 2 presents a few examples of all the 9577 images determined as outliers.

Metadata missing values were addressed by introducing a new parameter *unknown* for the sex, age, and anatomical location. In all, 3 sex features, 10 anatomical location features, and 19 sex features were encoded utilizing a straightforward One-Hot encoding procedure (Potdar et al., 2017). In this encoding, the matching attribute for each given output level is 1 while the remainder are all 0. A total of 32 stacked features are used as input for the patient-level data.

Data Augmentation: Three popular methodologies from the literature were evaluated in order to discover a suitable data augmentation regime for such real-world classification task; namely, AutoAugment (Cubuk et al., 2019), RandAugment (Cubuk et al., 2020) and AugMix (Hendrycks et al., 2020). Before a selection, an adaptation of the customized standard augmentation by (Ha et al., 2020) was studied in order to find the most suitable augmentation technique for newly unseen data.

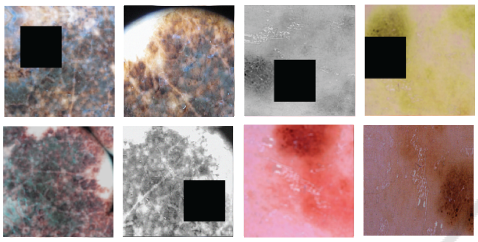

Figure 3: Image augmentation employed: a standard augmentation regime (random flip, rotation, brightness/contrast and blur/gaussian noise) followed by a random and resized crop strategy, CutOut of 30% image size, and gray and color-jitter/hue-saturation changes.

Figure 3 shows the augmentation regime used for all the models, which was based on the idea of avoiding the deconstruction of features and patterns in the melanocytic images described in the ABCD rule (Ali et al., 2020): where skin lesion asymmetry is a major indicator of malignant melanoma, in contrast to benign pigmented skin lesions, which are normally round and symmetric, melanomas spread uncontrollably. As a result, asymmetry, border, color, and diameter are critical in developing a skin lesions augmentation regime. Taking inspiration from Contrastive Learning (Chen et al., 2020) the composition of simple augmentations for learning good representations, gray and color distortions were adopted. Moreover, key to the locality of the augmentation was a heavy cropping strategy, where random resized crops were fed into the models followed by random brightness and contrast changes including color jitter, random flipping, random rotation, random scaling, and random blur/noise/sharpen changes. Furthermore, CutOut (Devries and Taylor, 2017) was used with one hole that was 30% the size of the image and had a 50% chance of appearing. Finally, a couple of augmentation strategies, including microscopy-crop and color constancy shades of grey as in (Gessert et al., 2020), were explored, but yielded no benefits and were therefore rejected.

Data Splitting: For the data splitting, the objective was to find a strategy that could work for both model selection and hyper-parameter optimization. The holdout method is the simplest strategy for evaluating a classifier and although it is not the best strategy to exhaustedly assess the models on the whole bulk of the data, it provides the advantage of immediate experiments to determine the fundamental settings for a robust classifier. To achieve generalization on previously unseen data, it was vital to verify that the training and validation were representative of the full dataset. Hence, a stratified split based on the skin lesion target class was necessary and based on the empirical findings, a 90% to 10% split was decided.

Following a data-driven approach, adding external data as in (Steppan and Hanke, 2021), demonstrated a slight improvement for the outlier class. Therefore, datasets described in Figure 4 (a) were used to feed the models in order to reach diversity in our ensemble. Moreover, in order to include metadata features, the ISIC 2019 and ISIC 2020 datasets were both used for training with a bulk of 57301 images. The stratified split can be inspected in Figure 4 (b).

3.3 Model Training with LR Scheduler and Selecting the Optimizer

We applied the procedure known as ”super-convergence” (Smith and Topin, 2019) in parallel throughout the whole model implementation, given our GPU and training time limitations. The ”One-Cycle” Learning Rate (LR) policy proposed in (Smith, 2018) makes use of this feature to address the stochastic aspect of NNs by oscillating the LR into greater and smaller values that aid in breaking out of a plateau or local minima regions of the loss functions. One cycle consists in two steps: one in which LR increases from minimum to maximum and the other in which it lowers from maximum to minimum of the total number of epochs. In super-convergence, networks are trained with high LRs in an order of magnitude fewer iterations and with better final test accuracy than when a constant training regime is used. Super-convergence depends critically on training with a single LR cycle and a high LR. Furthermore, AdamP optimizer has been shown to outperform the vast majority of Gradient Descent Based optimizers in both computational cost and performance on ImageNet (Heo et al., 2021). In (Smith, 2018), the authors suggested testing any of the $3e-4$, $1e-4$, and $3e-5$ as the maximum LR, and in order to have uniformity for all tests, $3e-4$ was selected as the max LR.

We used the automatic scoring system detailed in

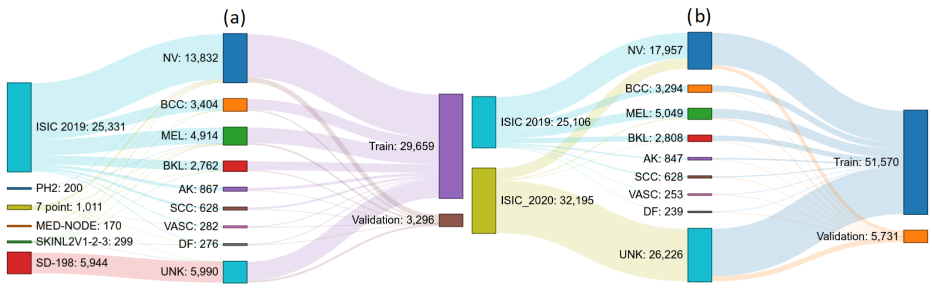

Figure 4: Skin Lesion Datasets Distribution for the external data is depicted in (a). It displays the 25,331 samples from the ISIC 2019 as well as the contributions from the remaining external datasets and also indicates the splitting made for training and validation. On the otther hand, (b) shows the metadata Skin Lesion Datasets Distribution for the 2019 and 2020 ISIC datasets with 32,196 additional images. The contribution in each class is demonstrated here, along with the splitting approach and 9:1 proportions for training and validation.

(Archive, 2019), for the 2019 ISIC Challenge to evaluate the performance of our models, Accuracy (ACC), Balanced Multi-class Accuracy (BACC), BACC of the validation set (Val BACC), sensitivity (SE), specificity (SP), Dice Coefficients (DI) and Area Under the Curve (AUC) scores, receive operating characteristics (ROC) curve.

3.4 Experimental Results

The results from the CNNs baseline in research (Steppan and Hanke, 2021) were adapted with the OneCycle LR, given training and computational constraints. Furthermore, a baseline of ViTs had to be obtained in order to have a first look and comparison between ViTs and CNNs in the skin lesion classification task. The CNNs that were used for baseline comprise the Efficient Nets (Tan and Le, 2019), Inception Resnet V2 (Szegedy et al., 2017) and ResNeXt (Xie et al., 2017). In the case of ViTs, we used as the baseline: the basic ViT (Dosovitskiy et al., 2021), BEiT (Bao et al., 2022), SwinT (Liu et al., 2021), and SwinTV2 (Liu et al., 2022a). Hence, the relevant models and their performance are displayed in Table 3. Furthermore, initially, only images from the whole dataset shown in Figure 4 were used. As a result, 29,639 training samples and 3296 validation images were used with a 90-10 split from the PH2, 7-point criterion, MED-NODE, SKINLV2-V1-2-3, SD-198, and ISIC 2019 datasets; melanoma had 4914 samples for baseline. With this particular setup, preliminary results show that CNNs defeat ViTs ensemble by a narrow margin. Additionally, the image size was multi-resolution, and the EfficientNet B5 received the highest score of 0.483; Nonetheless, a variety of input sizes for the ViTs backbones were needed in order to adequately examine the results since ViTs lacks the richness of scaled resolution.

Table 3: ISIC 2019 baseline scores. No data preprocessing, duplicates removal or imbalance handling was performed.

Method	# Params	Image size	Data usage	Val BACC	2019 Score
SWSL ResNeXt-101 32x4d (Yalniz et al., 2019)	54M	224	External	72.09%	0.429
Inception-ResNet-V2 (Szegedy et al., 2017)	56M	299	External	76.33%	0.433
EfficientNet B4 (Tan and Le, 2019)	19M	380	External	71.11%	0.424
EfficientNet B5 (Tan and Le, 2019)	30M	456	External	77.73%	0.483
CNNs baseline ensemble	0.496				
ViT-L-16 (Dosovitskiy et al., 2021)	304M	224	External	75.73%	0.418
Swin-L-4 (Liu et al., 2021)	197M	224	External	73.02%	0.464
SwinV2-B- (Liu et al., 2022a)	88M	256	External	74.56%	0.412
BeiT-B-16 (Bao et al., 2022)	87M	224	External	75.13%	0.403
ViTs baseline ensemble	0.482				

3.5 ViTs and CNNs Ensemble Results for 2019 ISIC Challenge

The 2019 ISIC Challenge, which contains an automatic scoring system and 8,239 challenging images in the test set, allowed for credibility in the evaluation of our model's generalization capabilities. The top network results, which were obtained through an ensemble of the ViTs and CNNs, are shown in Table 4. Although BEiT-L is a powerful network for the ImageNet dataset, as demostrated by (Bao et al., 2022), it underperformed in all of the test results from ViTs —with less than 0.500 for ISIC 2019 test score after thresholding— and hence was omitted.

Furthermore, the ensemble predictions were created using only the top six models from ViTs and CNNs. Although the 384 image size was best for the ViTs and the 380 image resolution was best for the CNNs, the multi-resolution technique for ensemble diversification allowed us to construct ensembles that outperformed all individual models ranging from 224 to 528. The DeiT-D3 achieved a top validation score of 91.73% and a high score of 0.593, indicating that it has captured features not present in the other mod-

Table 4: BACC on training in ViTs and CNNs state-of-the-art models. All hold-out splitting with 90 to 10% for training and validation. We considered a heavy cropping strategy with TTA 32 and only 10 epochs training via fine-tuning. Values are given in % as BACC validation. The ensemble was used as the average of all predictions from ViTs and CNNs models. External refers to both the 2019 dataset and the external datasets, and Meta means the 2019 dataset and 2020 datasets training both the images and metadata. In all cases, the 9 classes were used for prediction.

Method	# Params	Image size	Data usage	Val BACC	2019 Score
ViT-L-16 (Dosovitskiy et al., 2021)	26M	224	External Meta	78.35% 83.56%	0.514 0.527
VOLO-D3 (Yuan et al., 2022)	306M	512	External Meta	82.31% 85.36%	0.512 0.516
DeiT-D3 (Touvron et al., 2021a)	305M	384	External Meta	89.97% 91.73%	0.592 0.593
CaiT-M-36 (Touvron et al., 2021b)	271M	380	External Meta	84.29% 88.21%	0.571 0.589
Swin-L-4 (Liu et al., 2021)	197M	224	External Meta	81.17% 83.87%	0.526 0.564
Swin-L-V2 (Liu et al., 2022a)	197M	384	External Meta	86.10% 89.46%	0.563 0.610
ViTs Ensemble (ViTs above)	0.612				
SWSL ResNeXt-101 32x4d (Yalniz et al., 2019)	54M	224	External Meta	75.73% 74.06%	0.576 0.579
Inception-ResNet-V2 (Szegedy et al., 2017)	56M	299	External Meta	78.23% 78.24%	0.586 0.587
EfficientNet b4 NS (Xie et al., 2020)	19M	380	External Meta	83.66% 84.85%	0.603 0.630
EfficientNet b5 NS (Xie et al., 2020)	30M	456	External Meta	84.25% 85.94%	0,604 0.618
EfficientNet b6 NS (Xie et al., 2020)	43M	528	External Meta	85.99% 86.07%	0.612 0.630
ConvNeXt-B (Liu et al., 2022b)	89M	384	External Meta	85.91% 86.95%	0.592 0.594
CNNs Ensemble (CNNs above)	0.660				

Table 5: Ensemble method used for the ViTs and CNNs.

Ensemble method	ViTs ensemble 2019 Score	CNNs ensemble 2019 Score
Rank of probabilities	0.611	0.647
Majority voting	0.542	0.603
Averaging	0.612	0.660

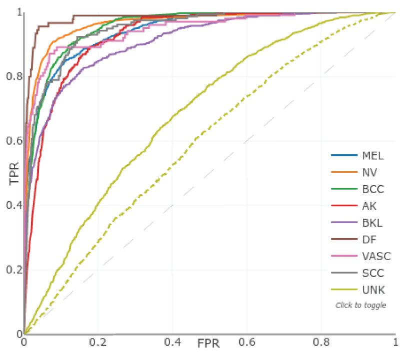

Figure 5: ROC curve with improvement AUC for the unknown class.

els. CNNs, on the other hand, outperform ViTs for the majority of individual ensembles in both external and meta data. Finally, it was not intended to utilize a brute force averaging strategy, as was the case in earlier 2019 and 2020 ISIC submissions, hence a model selection approach had to be used.

Table 6: Outlier class metrics comparison with the OOD results for the top 1 in the 2019 ISIC live challenge.

Metric	AUC	AUC Sens >80%	Average Precision
Unk	0.595	0.310	0.234
Unk-OOD	0.686	0.437	0.302

In order to take explicit care of OOD samples and outperform the current methods in the challenges, we used the modified Gram-OOD* to calculate the OOD samples, as described in Section 2.3. Table 6 depicts a comparison after the modified Gram-OOD* method was applied, accounting for a slight improvement in the AUC. We achieved AUC sensitivity higher than 80% and average precision of 0.686, 0.437 and 0.302, respectively. Finally, the outlier class improvement is shown in Figure 5. It illustrates the new ROC Curve for the UNK class, alongside a dashed line corresponding to the previous ROC Curve (a) from Figure 9. The rest of the classes remains the same as the modified Gram-OOD* only replacing the predictions from the outlier unknown class.

3.6 Model Selection

Once the previous results have achieved second place in the ISIC 2019 live leaderboard with the CNNs ensemble, the best models to enhance the ensemble for ViTs must be identified. The approach for determining the optimal ensemble is provided here, which entails assessing a gap between models using the correlation of training with test predictions for each model. Therefore, MCM, used by (Nikita Kozodoi, 2020), was extended in this study for the nine class predictions (see Section 2.2).

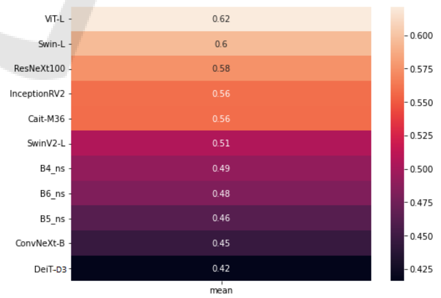

Figure 6: Mean correlation matrix of predictions for model selection. The greater gap means a poor model, likely overfitting local data.

Figure 6 illustrates the results gap generated to select the models of the ensemble. It is worth noting that the Deit-D3 appears to be among the most feature-rich model, with an overall gap of 0.42, followed by the ConvNext-B with 0.45. As a result, these two models were chosen for the ensemble; note that the EfficientNets with Noisy Student weights outperformed the ViTs in the task as a backbone; the B4, B5 and B6 gaps are the ones that follow with 0.46, 0.48 and 0.49, respectively. Finally, the remaining models were eliminated one by one, since it was determined that each one was degrading the total score.

3.7 ViTs and CNNs Final Ensemble

Table 8 represents the ensemble that reached first place in the 2019 ISIC live challenge and third place in the 2020 ISIC live challenge (Figures 7 and 8). It was composed of a diversification of models, both ViTs and CNNs in Table 4, and discriminated after a model selection with the MCM from section 3.6.

3.7.1 ISIC Submissions and Evaluation

We submitted our model to the ISIC Challenge submission system, which allows for automatic format validation and scoring. Figure 9 and Table 8 resume the results obtained from the unseen data for the 2019 Challenge and the 2020 ISIC challenge: (a) shows the ROC Curve result for each individual class in the 2019 challenge, and (b) shows the melanoma predictions results illustrated in the ROC Curve from the ISIC 2020 dataset.

A brief look at Figure 9 ROC curve and AUC reveals that the ROC curve performs much worse with the UNK class than with the other classes. Likewise from Table 8, all classes have an AUC greater than 0.9, with the exception of the outlier class, which has the lowest AUC of 0.595. Moreover, in the case of melanoma, the AUC from table 8 shows a competent score of 0.943 which motivated a submission in the 2020 ISIC challenge that assesses the malignant prediction. The ROC Curve (b) in Figure 9 and the metrics results in Table 7 are the results of the submission to the 2020 ISIC live challenge. The 0.940 AUC allowed the project to finish third in the 2020 ISIC live challenge, confirming the proposal's generalization capabilities in a different test dataset.

Furthermore, only the regular CE was employed in this experiment, which served to determine which

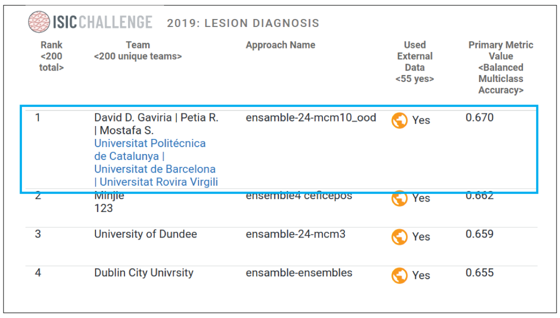
ISIC CHALLENGE 2019: LESION DIAGNOSIS

Rank <200 total>	Team <200 unique teams>	Approach Name	Used External Data <55 yes>	Primary Metric Value <Balanced Multiclass Accuracy>
1	David D. Gaviria | Petia R. | Mostafa S. Universitat Politécnica de Catalunya | Universitat de Barcelona | Universitat Rovira Virgili	ensamble-24-mcm10_ood	Yes	0.670
2	Minjie 123	ensemble4 cefcepos	Yes	0.662
3	University of Dundee	ensamble-24-mcm3	Yes	0.659
4	Dublin City Univrsity	ensamble-ensembles	Yes	0.655

Figure 7: First place in 2019 ISIC live leaderboard.

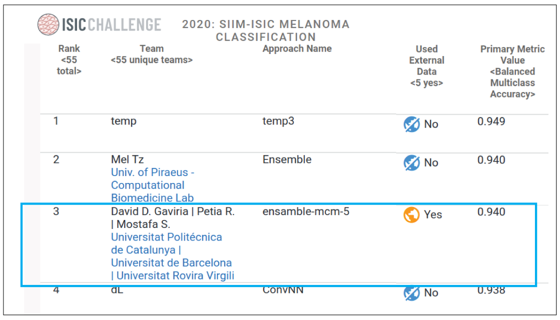
ISIC CHALLENGE 2020: SIIM-ISIC MELANOMA CLASSIFICATION

Rank <55 total>	Team <55 unique teams>	Approach Name	Used External Data <5 yes>	Primary Metric Value <Balanced Multiclass Accuracy>
1	temp	temp3	No	0.949
2	Mel Tz Univ. of Piraeus - Computational Biomedicine Lab	Ensemble	No	0.940
3	David D. Gaviria | Petia R. | Mostafa S. Universitat Politécnica de Catalunya | Universitat de Barcelona | Universitat Rovira Virgili	ensamble-mcm-5	Yes	0.940
4	dL	ConvNN	No	0.938

Figure 8: Third place in 2020 ISIC live leaderboard.

augmentation strategy works best; the same behaviour was observed by each one of the individual models. Following the criteria from the melanoma ABCD rule (Kasmi and Mokrani, 2016), our Adapted Augmentation regime produced the best overall results, with a greater Val BACC of 78.23% and 81.17% and an overall score of 0.462 and 0.479 for the Inception-Resnet-V2 and Swin-L-4, respectively. As a result, for all subsequent steps, this data augmentation regime was used.

3.8 Study on the Modified Gram-OOD*

The purpose of this experiment was to assess the improvement that was yielded using the layer-wise correlations compared to the activations of the Gram-OOD* method from (Pacheco et al., 2020). Results showed a significant improvement worth noting given the reduced computational cost (10 epochs). Table 9 shows the feature maps extracted from the activation and convolutional layers, respectively.

3.9 Study on the Loss Functions

The purpose of this experiment was to show the thresholding approach to treat better the imbalanced data compared to WCE. Moreover, since in many papers, Focal loss (FL) becomes well popular (Lin et al., 2020), we compare our loss function to it too. Using two of the ensemble models; the Swin-L ViT and Inception-Resnet-V2 representing CNNs; similar behaviour was observed on the rest of the models. Then, table 10 compares the results of the assessed loss functions to determine which approach among them for dealing with imbalanced datasets in skin lesion classification performs best.

The tests were carried out using the two kinds of networks from the preceding section, both CNNs and ViTs. These show that thresholding beats the other two by a significant margin, ranging from 0.013 and 0.022 with the WCE to 0.005 and 0.009 with FL the 2019 challenge score. Thus, the thresholding strategy

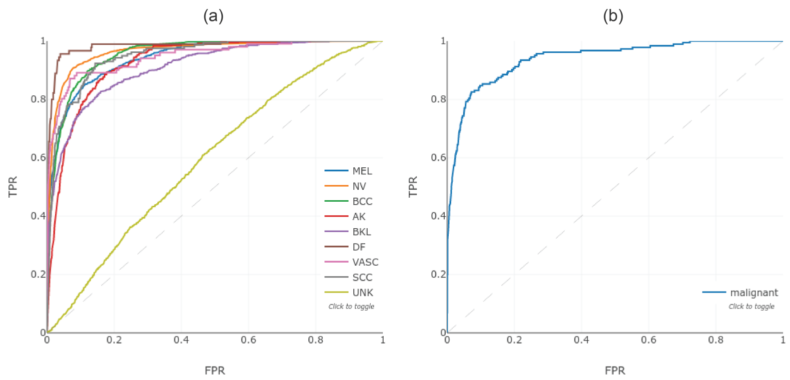

Figure 9: ROC curve for (a) the 0.670 BACC ensemble for the 2019 ISIC Challenge and (b) the melanoma with 0.940 AUC for the 2020 ISIC Challenge.

Table 7: Ensemble melanoma metrics for top-3 in the 2020 ISIC live challenge.

Metric	AUC	AUC Sens >80%	Average Precision	Accuracy	Sensitivity	Specificity	Dice Coefficient	PPV	NPV
MEL	0.940	0.899	0.544	0.982	0.284	0.999	0.426	0.852	0.983

Table 8: Ensemble metrics for top-1 in the 2019 ISIC.

Metrics	Mean	Diagnosis Category								
		MEL	NV	BCC	AK	BKL	DF	VASC	SCC	UNK
AUC	0.908	0.943	0.965	0.955	0.928	0.911	0.983	0.947	0.949	0.595
AUC, Sens >80%	0.836	0.892	0.943	0.915	0.861	0.820	0.975	0.918	0.887	0.310
Average Precision	0.597	0.821	0.938	0.774	0.404	0.640	0.608	0.572	0.382	0.234
Accuracy	0.928	0.913	0.910	0.918	0.931	0.937	0.986	0.981	0.972	0.808
Sensitivity	0.589	0.658	0.797	0.788	0.610	0.490	0.733	0.653	0.573	0.00
Specificity	0.972	0.965	0.964	0.938	0.948	0.979	0.989	0.985	0.981	1.00
Dice Coefficient	0.538	0.719	0.851	0.716	0.474	0.572	0.559	0.482	0.471	0.00
PPV	0.630	0.791	0.913	0.655	0.388	0.688	0.452	0.382	0.400	1.00
NPV	0.948	0.933	0.908	0.967	0.978	0.953	0.997	0.995	0.991	0.808

Table 9: Comparison of the usage of convolutional layers vs the activation functions as feature maps.

Method	TNR	AUC	DTACC
Gram-OOD* (Pacheco et al., 2020)	7.028	45.456	51.311
Modified Gram-OOD* (Ours)	9.226	59.414	57.083

Table 10: Comparisom of different loss functions. Thresholding was applied to the 2019 Score.

Imbalanced method	Model	Metric	
		Val BACC	2019 Score
Weighted Cross Entropy (Aurelio et al., 2019)	Inception-Resnet-V2 Swin-L-4	77.75% 80.63%	0.502 0.504
Focal Loss (Lin et al., 2020)	Inception-Resnet-V2 Swin-L-4	78.03% 80.94 %	0.509 0.515
CE with thresholding (Ours)	Inception-Resnet-V2 Swin-L-4	78.23% 81.17%	0.514 0.526

was adopted after the predictions, implying that the CE had to be used as a loss function for training, and thresholding was applied at the inference phase.

3.10 Discussion

When classifying skin lesions, especially in melanoma appearance, it is important to consider both the augmentation distortions and the patient's context (Strzelecki et al., 2021). When viewed alongside the images, the metadata has proven significant in every case. Moreover, an augmentation scheme that alters a skin mole to resemble a melanoma, especially when combined with elastic asymmetric transformations or grid distortions, may seriously hinder the NN learning capabilities.

4 CONCLUSIONS

Based on the diagnosis of skin lesions and recent publications, two open live challenges—ISIC 2019 and ISIC 2020— were used to study the classification of dermatological images and validate the overall performance of the DL solutions. Our study proves that no single model, nor ViTs neither CNNs could achieve a higher standing in both the 2019 and 2020 ISIC live challenges. Our ensemble of ViTs and CNNs was able to provide a huge diversity, necessary to achieve top-1 for the ISIC 2019 live challenge with a BACC of 0.670, and top-3 for melanoma classification in the ISIC-2020 live challenge with an AUC score of 0.940.

Additionally, we used the same target prediction for the malignant melanoma, indicating strong generalization potential to close the gap in considering deep learning techniques as a reliable source for an early diagnosis. Although the data used here mixed dermoscopy and clinical images, further research is required to assess the behavior of a DL solution with a bulk of clinical images in the test set. Despite improvements made in the topic of outliers, both for the data-driven approach and from the modified Gram-

OOD* adaptation, the OOD samples present in the 2019 ISIC remain an open challenge and further research on the topic is required to improve OOD detection for both CNNs and ViTs.

The ideal use for this technology would be a mobile app or online diagnostic tool that offers practical, prompt advise of whether a patient should consult a doctor about a worrisome lesion. To get close to that, a demo created along with further details may be found at: https://skin-lesion-diagnosis.web.app/.

ACKNOWLEDGEMENTS

This work was partially funded from the European Union's Horizon 2020 MUSAE project, Erasmus+ project RoboSteam, Acció Nuclis project DeepSens, and CERCA Programme / Generalitat de Catalunya. B. Nagarajan acknowledges the support of FPI Becas, MICINN, Spain. We acknowledge the support of NVIDIA Corporation with the donation of the Titan Xp GPUs.

REFERENCES

ACS, A. C. S. (2022). Key statistics for melanoma skin cancer. https://www.cancer.org/cancer/melanoma-skin-cancer/about/key-statistics.html. Accessed: 2022-08-30.

Ali, D. A.-R., Li, J., and O'Shea, S. J. (2020). Towards the automatic detection of skin lesion shape asymmetry, color variegation and diameter in dermoscopic images. *PLoS ONE*, 15.

Archive, I. (2019). Evaluation score. https://challenge.isic-archive.com/landing/2019/. Accessed: 2022-06-30.

Aurelio, Y. S., de Almeida, G. M., de Castro, C. L., and de Pádua Braga, A. (2019). Learning from imbalanced data sets with weighted cross-entropy function. *Neural Processing Letters*, 50:1937–1949.

Bao, H., Dong, L., and Wei, F. (2022). Beit: Bert pre-training of image transformers. *ArXiv*, abs/2106.08254.

Belilovsky, E., Eickenberg, M., and Oyallon, E. (2019). Greedy layerwise learning can scale to imagenet. *ArXiv*, abs/1812.11446.

Buda, M., Maki, A., and Mazurowski, M. A. (2018). A systematic study of the class imbalance problem in convolutional neural networks. *Neural networks : the official journal of the International Neural Network Society*, 106:249–259.

Chang, W.-Y., Huang, A., Yang, C.-Y., Lee, C.-H., Chen, Y.-C., Wu, T.-Y., and Chen, G.-S. (2013). Computer-aided diagnosis of skin lesions using conventional digital photography: A reliability and feasibility study. *PLoS ONE*, 8.

Chen, J., Chen, J., Zhou, Z., Li, B., Yuille, A. L., and Lu, Y. (2021). Mt-transunet: Mediating multi-task tokens in transformers for skin lesion segmentation and classification. *ArXiv*, abs/2112.01767.

Chen, T., Kornblith, S., Norouzi, M., and Hinton, G. E. (2020). A simple framework for contrastive learning of visual representations. *ArXiv*, abs/2002.05709.

Combalia, M., Codella, N. C. F., Rotemberg, V. M., Helba, B., Vilaplana, V., Reiter, O., Halpern, A. C., Puig, S., and Malvehy, J. (2019). Bcn20000: Dermoscopic lesions in the wild. *ArXiv*, abs/1908.02288.

Cubuk, E. D., Zoph, B., Mané, D., Vasudevan, V., and Le, Q. V. (2019). Autoaugment: Learning augmentation strategies from data. *2019 IEEE/CVF CVPR*, pages 113–123.

Cubuk, E. D., Zoph, B., Shlens, J., and Le, Q. V. (2020). Randaugment: Practical automated data augmentation with a reduced search space. *2020 IEEE/CVF CVPRW*, pages 3008–3017.

Devries, T. and Taylor, G. W. (2017). Improved regularization of convolutional neural networks with cutout. *ArXiv*, abs/1708.04552.

Dosovitskiy, A., Beyer, L., Kolesnikov, A., Weissenborn, D., Zhai, X., Unterthiner, T., Dehghani, M., Minderer, M., Heigold, G., Gelly, S., Uszkoreit, J., and Houlsby, N. (2021). An image is worth 16x16 words: Transformers for image recognition at scale. *ArXiv*, abs/2010.11929.

Forsea, A. M. (2020). Melanoma epidemiology and early detection in europe: Diversity and disparities. *Dermatology practical & conceptual*, 10 3:e2020033.

Gessert, N., Nielsen, M., Shaikh, M., Werner, R., and Schlaefer, A. (2020). Skin lesion classification using ensembles of multi-resolution efficientnets with meta data. *MethodsX*, 7.

Giotis, I., Molders, N., Land, S., Biehl, M., Jonkman, M. F., and Petkov, N. (2015). Med-node: A computer-assisted melanoma diagnosis system using non-dermoscopic images. *Expert Syst. Appl.*, 42:6578–6585.

Ha, Q., Liu, B., and Liu, F. (2020). Identifying melanoma images using efficientnet ensemble: Winning solution to the siim-isic melanoma classification challenge. *ArXiv*, abs/2010.05351.

Hendrycks, D., Mu, N., Cubuk, E. D., Zoph, B., Gilmer, J., and Lakshminarayanan, B. (2020). Augmix: A simple data processing method to improve robustness and uncertainty. *ArXiv*, abs/1912.02781.

Heo, B., Chun, S., Oh, S. J., Han, D., Yun, S., Kim, G., Uh, Y., and Ha, J.-W. (2021). Adamp: Slowing down the slowdown for momentum optimizers on scale-invariant weights. *arXiv: Learning*.

Kasmi, R. and Mokrani, K. (2016). Classification of malignant melanoma and benign skin lesions: implementation of automatic abcd rule. *IET Image Process.*, 10:448–455.

Liang, S., Li, Y., and Srikant, R. (2018). Enhancing the reliability of out-of-distribution image detection in neural networks. *arXiv: Learning*.

Lin, T.-Y., Goyal, P., Girshick, R. B., He, K., and Dollár, P. (2020). Focal loss for dense object detection. *IEEE Transactions on Pattern Analysis and Machine Intelligence*, 42:318–327.

Liu, Z., Hu, H., Lin, Y., Yao, Z., Xie, Z., Wei, Y., Ning, J., Cao, Y., Zhang, Z., Dong, L., Wei, F., and Guo, B. (2022a). Swin transformer v2: Scaling up capacity and resolution. *IEEE/CVF CVPR*, pages 11999–12009.

Liu, Z., Lin, Y., Cao, Y., Hu, H., Wei, Y., Zhang, Z., Lin, S., and Guo, B. (2021). Swin transformer: Hierarchical vision transformer using shifted windows. *2021 IEEE/CVF ICCV*, pages 9992–10002.

Liu, Z., Mao, H., Wu, C., Feichtenhofer, C., Darrell, T., and Xie, S. (2022b). A convnet for the 2020s. pages 11976–11986.

Nikita Kozodoi, Gilberto Titericz, H. G. (2020). 11th place solution writeup. https://www.kaggle.com/competitions/siim-isic-melanoma-classification/discussion/175624. Accessed: 2022-04-30.

Pacheco, A. G. C., Sastry, C. S., Trappenberg, T. P., Oore, S., and Krohling, R. A. (2020). On out-of-distribution detection algorithms with deep neural skin cancer classifiers. *IEEE/CVF CVPRW*, pages 3152–3161.

Potdar, K., Pardawala, T. S., and Pai, C. D. (2017). A comparative study of categorical variable encoding techniques for neural network classifiers. *International Journal of Computer Applications*, 175:7–9.

Richard, M. D. and Lippmann, R. (1991). Neural network classifiers estimate bayesian a posteriori probabilities. *Neural Computation*, 3:461–483.

Rotemberg, V. M., Kurtansky, N. R., Betz-Stablein, B., Caffery, L. J., Chousakos, E., Codella, N. C. F., Combalia, M., Dusza, S. W., Guitera, P., Gutman, D., Halpern, A. C., Kittler, H., Köse, K., Langer, S. G., Liopryis, K., Malvehy, J., Musthaq, S., Nanda, J., Reiter, O., Shih, G., Stratigos, A. J., Tschandl, P., Weber, J., and Soyer, H. P. (2021). A patient-centric dataset of images and metadata for identifying melanomas using clinical context. *Scientific Data*, 8.

Russakovsky, O., Deng, J., Su, H., Krause, J., Satheesh, S., Ma, S., Huang, Z., Karpathy, A., Khosla, A., Bernstein, M. S., Berg, A. C., and Fei-Fei, L. (2015). Imagenet large scale visual recognition challenge. *International Journal of Computer Vision*, 115:211–252.

Sarker, M. M. K., Moreno-García, C. F., Ren, J., and Elyan, E. (2022). Transslc: Skin lesion classification in dermatoscopic images using transformers. In *Annual Conference on Medical Image Understanding and Analysis*, pages 651–660. Springer.

Sastry, C. S. and Oore, S. (2019). Detecting out-of-distribution examples with in-distribution examples and gram matrices. *ArXiv*, abs/1912.12510.

Shanmugam, D., Blalock, D. W., Balakrishnan, G., and Guttag, J. V. (2020). When and why test-time augmentation works. *ArXiv*, abs/2011.11156.

Smith, L. N. (2018). A disciplined approach to neural network hyper-parameters: Part 1 - learning rate, batch size, momentum, and weight decay. *ArXiv*, abs/1803.09820.

Smith, L. N. and Topin, N. (2019). Super-convergence: very fast training of neural networks using large learning rates. In *Defense + Commercial Sensing*.

Steppan, J. and Hanke, S. (2021). Analysis of skin lesion images with deep learning. *ArXiv*, abs/2101.03814.

Strzelecki, M., Strakowska, M., Kozłowski, M., Urbańczyk, T., Wielowieyska-Szybińska, D., and Kociolek, M. (2021). Skin lesion detection algorithms in whole body images. *Sensors (Basel, Switzerland)*, 21.

Sun, X., Yang, J., Sun, M., and Wang, K. (2016). A benchmark for automatic visual classification of clinical skin disease images. In *ECCV*.

Szegedy, C., Ioffe, S., Vanhoucke, V., and Alemi, A. A. (2017). Inception-v4, inception-resnet and the impact of residual connections on learning. In *AAAI*.

Tan, M. and Le, Q. V. (2019). Efficientnet: Rethinking model scaling for convolutional neural networks. *ArXiv*, abs/1905.11946.

Touvron, H., Cord, M., Douze, M., Massa, F., Sablayrolles, A., and J'egou, H. (2021a). Training data-efficient image transformers & distillation through attention. In *ICML*.

Touvron, H., Cord, M., Sablayrolles, A., Synnaeve, G., and J'egou, H. (2021b). Going deeper with image transformers. *2021 IEEE/CVF ICCV*, pages 32–42.

Tschandl, P., Rosendahl, C., and Kittler, H. (2018). The ham10000 dataset, a large collection of multi-source dermatoscopic images of common pigmented skin lesions. *Scientific Data*, 5.

Vaswani, A., Shazeer, N. M., Parmar, N., Uszkoreit, J., Jones, L., Gomez, A. N., Kaiser, L., and Polosukhin, I. (2017). Attention is all you need. In *NIPS*.

Walter, F. M., Prevost, A. T., Vasconcelos, J. C., Hall, P., Burrows, N. P., Morris, H. C., Kinmonth, A. L., and Emery, J. D. (2013). Using the 7-point checklist as a diagnostic aid for pigmented skin lesions in general practice: a diagnostic validation study. *The British journal of general practice : the journal of the Royal College of General Practitioners*, 63 610:e345–53.

WHO, W. H. O. (2017). Radiation: Ultraviolet (uv) radiation and skin cancer. https://www.who.int/news-room/questions-and-answers/item/radiation-ultraviolet-(uv)-radiation-and-skin-cancer. Accessed: 2022-06-30.

Xie, Q., Hovy, E. H., Luong, M.-T., and Le, Q. V. (2020). Self-training with noisy student improves imagenet classification. *IEEE/CVF CVPR*, pages 10684–10695.

Xie, S., Girshick, R. B., Dollár, P., Tu, Z., and He, K. (2017). Aggregated residual transformations for deep neural networks. *IEEE CVPR*, pages 5987–5995.

Yalniz, I. Z., Jégou, H., Chen, K., Paluri, M., and Mahajan, D. K. (2019). Billion-scale semi-supervised learning for image classification. *ArXiv*, abs/1905.00546.

Yuan, L., Hou, Q., Jiang, Z., Feng, J., and Yan, S. (2022). Volo: Vision outlooker for visual recognition. *IEEE Trans. PAMI*, PP.